Application of Thin Films to Porous Mineral Oxides Using Two-Dimensional Solvents

Thin polymeric films have been applied to the surface of a porous material in a novel process. Nitrogen sorption, a conventional tool for measuring surface areas and pore size distributions, can be employed for determining the thickness of such films through a comparison of the pore size distribution curves before and after film formation. The thickness of a polystyrene film on a porous alumina powder is determined and compared with the theoretical thickness for styrene polymerized inside a two-dimensional solvent, which consists of a partial bilayer of sodium dodecyl sulfate physically adsorbed from an aqueous solution onto the powder. Film thicknesses ranged from 1.8 to 0.4 nm while BET surface area decreased from 94.7 to 57.8 m^2/g. The powder surface changes from hydrophilic to hydrophobic while retaining the basic pore structure.

Jengyue Wu, Jeffrey H. Harwell, Edgar A. O'Rear
Institute for Applied Surfactant Research
and
Department of Chemical Engineering
and Materials Science
University of Oklahoma
Norman, OK 73019

Sherril D. Christian
Institute for Applied Surfactant Research
and
Department of Chemistry
University of Oklahoma
Norman, OK 73019

Introduction

A novel three-step process for the formation of ultrathin polymer films on solid surfaces has been demonstrated using such common materials as alumina powders, sodium dodecyl sulfate, styrene, and sodium persulfate. Hybrid materials formed with this new technology might readily be utilized as chromatographic packings, inorganic-core ion exchange resins, or as a substrate for immobilized hydrophobic enzymes. Moreover, the unique reaction conditions might yield polymers of unusual molecular structure and molecular weight distribution. In this paper, films formed by this process on a porous powder are characterized by analysis of the surface area and pore size distribution of the powder before and after the formation of the thin film.

As shown in Figure 1, the process can be envisioned as occurring in three major steps. The first step is the formation of an admicelle (Harwell et al., 1985), by the adsorption of a surfactant bilayer at the solid/aqueous solution interface. An admicelle may be considered to be the surface analogue of a micelle. The second step involves the solubilization of a monomer into the bilayer, a phenomenon called adsolubilization, which may be conveniently thought of as a surface analogue of the solubilization of organic materials by surfactant micelles. In the partitioning of the monomer into the bilayer, the surfactant aggregate acts as a two-dimensional solvent to concentrate the monomer at the surface. The third step is the polymerization of the monomer inside the two-dimensional solvent. Details of the reaction conditions used in the formation of the ultrathin film characterized in this paper were published elsewhere (Wu et al., 1987a, b, c). As an introduction, the three steps of the novel film-forming process are discussed and evidence for film formation is reviewed briefly here in terms of the specific system selected for this study.

Correspondence concerning this paper should be addressed to E. A. O'Rear.

Thin Film Formation by Polymerization Inside a Two-Dimensional Solvent

Step 1. Admicelle formation

The patchwise distribution of surfactant aggregates formed locally on the surface through adsorption from an aqueous solution (admicelles) is a well-known phenomenon in the literature. Using the known surface area of the alumina powder chosen for this study, and literature values of the cross-sectional area for the head group of a sodium dodecyl sulfate (SDS) molecule, it was deduced that a partial surfactant bilayer was produced under the reaction conditions. While SDS will not adsorb to form admicelles on alumina under all conditions, surface aggregate formation may be induced at surfactant concentrations below the critical micelle concentration (CMC) of the surfactant by manipulation of the solution pH and counterion concentration (Scamehorn et al., 1982). To obtain admicelle formation, the most critical parameter to be manipulated is the

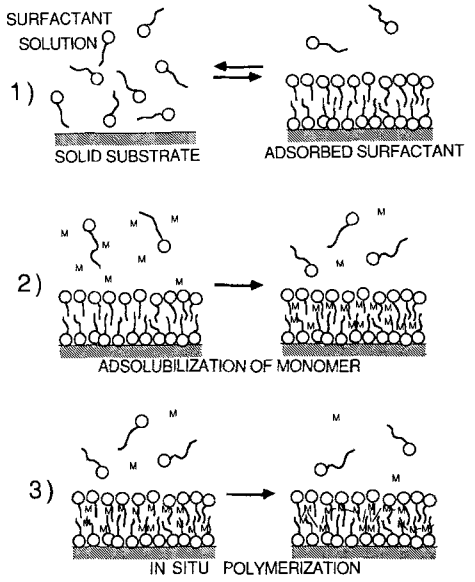

Figure 1. Formation of a thin film by polymerization in a two-dimensional solvent.

solution pH, relative to the pH at which the oxide exhibits a net surface charge of zero (referred to as the point of zero charge, or PZC). At pH values below the PZC, the surface becomes protonated and more positively charged; above the PZC the surface is negatively charged. Consequently, anionic surfactants adsorb below the PZC and cationic surfactants above. In our study, the alumina powder had a measured PZC of pH 9.5 at 30°C. Because an anionic surfactant was chosen to form the bilayer, the pH of the solution from which the surfactant was adsorbed was adjusted to low pH, arbitrarily pH 4. With sufficient surfactant, this level of acidity assures a highly charged surface and formation of a complete bilayer at the interface.

Step 2. Monomer adsolubilization

Under conditions favorable for the formation of admicelles and unfavorable for the presence of micelles in an aqueous system, hydrophobic species are concentrated at the interface in a phenomenon called adsolubilization. As a prelude to the film-forming polymerization reaction (step 3), hydrophobic monomer is adsolubilized or partitioned into the adsorbed surfactant aggregates of step 1.

The following summary of experimental observations supports adsolubilization as a key step in film formation. Concentration changes of monomer (i.e., styrene) in the supernatant, as measured by HPLC, have demonstrated the partitioning of styrene into the admicelles. For this particular system, care was necessarily taken that no liquid monomer be present; that is, all styrene was in the form of either dissolved monomer in the aqueous phase or adsolubilized in sodium dodecyl sulfate admicelles. In the absence of surfactant, no adsorption of monomer could be detected. In the presence of the adsorbed surfactant with sufficient driving force, styrene adsolubilization was observed to occur at a nearly constant adsorbed SDS to adsolubilized styrene molecular ratio of 2:1, suggestive of an ordered structure. To attain this saturation of the bilayer, it was necessary to increase the solubility of the styrene in the supernatant by adding cosolvent ethanol.

Because the monomer of this system is quite volatile, both the adsolubilization and subsequent reaction steps were carried out in sealed vials. A mass balance showed that monomer which disappeared from the supernatant during this preequilibration step was later recoverable in the form of polymer by extraction of the modified powder with a suitable solvent for polystyrene. A kinetic study revealed that further adsolubilization of monomer occurs as the polymerization step proceeds.

Step 3. Polymerization of adsolubilized monomer

Beyond the purpose of concentrating monomer at the surface of the substrate, the admicelles function as reaction loci or as a two-dimensional reaction solvent for the polymerization. Initiators begin the formation of polymer, probably by mechanisms similar to those occurring in conventional emulsion techniques. In this case, sodium persulfate was added to the supernatant, followed by heating the sealed vial with the equilibrated solution and alumina of step 2 to 60°C. Persulfate is a water-soluble initiator, so the polymerization proceeds through electron transfer or partitioning of radicals formed in the aqueous supernatant into the surfactant layer. Styrene polymer was recovered by tetrahydrofuran extraction of the isolated alumina after the reaction step, with intermediate washings, if necessary, by deionized water, followed by drying in a vacuum at a temperature below the boiling point of styrene. Comparison of the UV spectrum for the extract with those of known samples of polystyrene confirmed the conversion of monomer to polymer as a function of reaction time. Fourier transform infrared (FTIR) spectra not only showed the presence of polystyrene and SDS on the alumina surface, but also showed the emergence of characteristic polystyrene peaks with reaction time, following the induction period observed for free radical polymerization.

Film thicknesses were measured by ellipsometry by forming the films, at conditions determined from studies on the powdered alumina, on oxide layers formed on aluminum that had been vacuum deposited to a thickness of 100 nm on glass slides. After washing the slides, no films were detected for short reaction times; however, following an induction time, films of 3.4 to 3.6 nm were measured on the slides. For very long reaction times the measured films were as thick as 13 nm, consistent with the observation of continued monomer partitioning into the bilayer during the reaction.

Determination of Pore Size Distributions

Nitrogen sorption is a widely adopted method for examining the structural character of porous materials. Experimentally, the amount of gas adsorbed or condensed at low temperature is measured as a function of the relative pressure (partial pressure of nitrogen divided by the saturation pressure). An isotherm for the unmodified high surface area alumina powder is shown in Figure 2. At low relative pressures, data can often be interpreted by BET analysis, yielding estimates of surface area and C, a parameter equal to the ratio of equilibrium constants for the adsorption of first and subsequent layers. As a result of Laplace pressure contributions, higher relative pressures of values 0.4–1.0 cause condensation below the saturation pressure. Relating curvature of the interface to pore dimensions and determining the volume of condensed nitrogen as a function of the relative pressure provide information on the internal volume filled for pores of various sizes. From this, one can infer a pore size distribution.

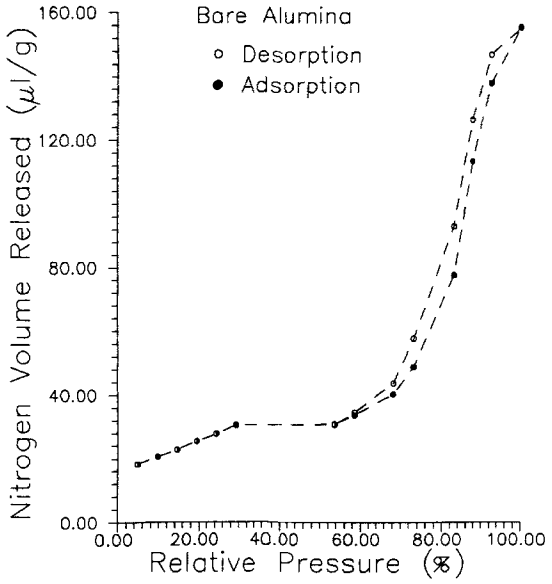

Figure 2. Nitrogen sorption isotherm for unmodified alumina.

There are two models used frequently in calculating pore size distributions. Both models, the cylindrical pore model and the slit-shaped (or parallel-plate) model, assume specific pore shapes, which makes the calculation of the pore surface area possible. Without the assumption of a pore shape, the pore surface area cannot be estimated from the discrete pore volume only. It is the latter quantity that is measured experimentally, as a function of the relative pressure.

The phenomena of multilayer adsorption (or desorption) and pore condensation (or evaporation) occur simultaneously at a relative pressure greater than 0.3 to 0.4. Pore sizes can be calculated based on sorption isotherms by manipulating the dependence of adsorbed thickness and pore radius (or width) on the relative pressure. Two independent methods have been introduced: one is the isotherm method of Wheeler (1951), the other is the mercury porosimetry method of Drake (1945). The isotherm method was further developed by many workers for both the cylindrical pore model (Outlon, 1948; Barrett et al., 1951; Cranston and Inkley, 1957; Joyner et al., 1951; Wayne, 1951; Pierce and Smith, 1950; Pierce, 1953; Dubinin, 1980; Juhola and Edwin, 1949), and the slit-shaped pore models (Ries et al., 1945; Innes, 1957).

Despite so much effort devoted by these workers to elucidating the structures of porous particles from nitrogen sorption data, the contribution of the adsorbed layer thickness was not recognized as a key variable in these analyses until the 1960's. The incorporation of the adsorption potential was first formulated by Deryagin. This, however, did not receive much attention from others. It was not until later that de Boer and coworkers (1964a, b, 1965a, b) systematically established an integrated treatment of pore size distributions that included the adsorption potential of the adsorbent surface into the analysis of pore structures.

Calculation of Pore Size Distributions

For the de Boer ideal cylindrical pore model, the thickness of the adsorbed layer of gas molecules, and thus the effective pore radius which determines the onset of capillary condensation in the pore, is a function of both the actual pore radius and the relative pressure. Calculations of the pore distribution from the capillary condensation or evaporation data thus also allow for thinning of the adsorbed gas multilayer as a function of pore radius and relative pressure. The necessity of accounting for this phenomenon in the analysis of the sorption data has been demonstrated by de Boer and others. This complicates the numerical analysis of the data; at each successive relative pressure, the radii of pores not filled with gas condensate must be corrected for the thickness of the adsorbed gas multilayer. The common BET analysis of gas sorption data does not account for this phenomenon, but there is an abundant literature which describes the application of the de Boer analysis to systems of the type studied here. Details of the procedure used here are available elsewhere (Roberts, 1967; Christian and Tucker, 1981a, b; Wu, 1987).

Determination of Thin-Film Thickness Inside Alumina Pores

For films formed on flat surfaces, ellipsometry is the obvious method for determining the thickness of thin films. In this paper, the thickness of a film formed on the surface of a porous alumina powder is estimated by comparing the pore size distribution of the powder before and after the formation of the film. It will be seen that the only explanation for the change in pore size distribution observed to occur after the polymerization reaction is the formation of an ultrathin film inside the porous structure of the alumina; the nitrogen sorption studies indicate that both the surface area and the pore size distribution are largely unchanged by the film-forming process. Yet, after the film has been applied, the alumina surface can be changed from hydrophilic to hydrophobic simply by washing it with water; this is discussed in detail below.

Our determination of the ultrathin film thickness inside the alumina pores by means of the nitrogen sorption isotherms starts with the results of the pore size distribution analyses for the bare alumina and for the alumina with the thin film. Three distribution curves are calculated for the cylindrical pore model: pore volume, pore area, and total pore length distributions. A simple relation exists relating the pore sizes before and after the formation of ultrathin films inside the pores.

From the pore volume distributions, the film thickness may be determined by

$$t_f = r[1 - (V_c'/V_c)^{1/2}] \tag{1}$$

or alternatively,

$$V_c'/V_c = [(r - t_f)/r]^2 \tag{2}$$

From the pore surface area distributions, the film thickness is expressed by

$$t_f = r(1 - A_c'/A_c) \tag{3}$$

or equivalently,

$$A_c'/A_c = (r - t_f)/r \tag{4}$$

where

V_c' = pore volume for sample with film
V_c = pore volume for bare alumina
A_c' = pore surface area sample with film
A_c = pore surface area for bare alumina
r = pore radius
t_f = thickness of ultrathin film inside pores

The application of the above equations to the evaluation of film thickness is based on the assumption that the total pore length for a specific pore size is constant even after the film formation. This analysis is similar to the treatment developed by de Boer in calculating the effect of multilayer thinning on the gas sorption data. With this assumption, the film thickness can be estimated by drawing tie lines between the two distribution curves. The slopes of the tie lines can be inferred from Eq. 1 to 4. The slope of the tie lines between the total pore length distribution curves is zero, which makes the analysis for this case particularly simple.

Experimental Details

The alumina powder was purchased from Alfa Co. The original pellets, of 3.2 mm dia., were broken in a mortar and pestle into smaller particles. Using standard sieves, the alumina powders were screened and a 45–75 μm dia. powder sample was chosen for the pore volume distribution and BET surface area measurements. A Micromeritic Flowsorb 2300 instrument was used to run the nitrogen sorption experiments. Detailed procedures described in the manufacturer's equipment manual were followed.

Two kinds of alumina powders were used in this study. One was the original or bare alumina, the other was the modified alumina with the ultrathin films formed inside the pores. The latter sample was prepared by the method described in the Introduction, with a polymerization reaction time of 45 min. The concentrations of all the components were the same as given in previous papers (Wu et al., 1987a, b), except that the ratio of the weight of alumina to the solution volume was set at 0.20 g to 15 mL. A desorption branch and an adsorption branch were obtained for each sample for nitrogen/helium gas mixtures varying from 95 to 5% nitrogen.

Results and Discussion

The experimental nitrogen sorption isotherms of both the bare alumina and the alumina sample with the film are plotted in Figures 2 and 3. At low relative pressures, below 0.3, corresponding to the region of multilayer adsorption before the onset of capillary condensation, the data of the sorbed volume vs. the relative pressure are quite linear. Beginning at a relative pressure of 0.3, a rather flat region is followed by the hysteresis loop, which begins to emerge at a relative pressure of about 0.5. This loop reflects the irreversible work that cannot be recovered through the adsorption and desorption process, and is a consequence of the capillary condensation phenomenon. Meniscus effects associated with the capillary condensation and evaporation processes and the internal pore geometry are undoubtedly responsible for the existence of the hysteresis loop. The shape of the hysteresis loop is indicative of the shape of the pores, there being a significant difference in loops associated with the distribution of cylindrical pores and loops associated with a distribution of slit-shaped pores. Compared with the prediction of the

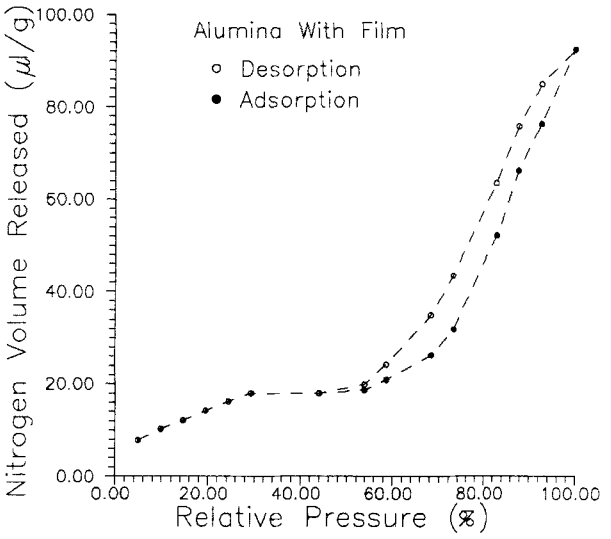

Figure 3. Nitrogen sorption isotherm for modified alumina.

loop gap from de Boer's theory, illustrated in Figure 4, it is apparent that the loops in the present systems are characteristic of a cylindrical pore distribution. Thus, the cylindrical pore model has been chosen as the basis for the subsequent pore size distributions for both samples.

Both alumina samples give a similar variation of the volume released vs. the relative pressure, except that the volume is smaller for the alumina with the film samples. The BET surface area determinations are plotted in Figure 5, along with a least-squares fit of the data. The bare alumina has a BET surface area of 94.7 m^2/g and a C value of 59; the BET area of the alumina with the film has been reduced to 57.8 m^2/g surface area and it has a C value of 22. The only difference between these two samples is the ultrathin film formed by the two-dimensional polymerization reactions for styrene. The decrease of BET surface area is around 40% of the original BET surface area. It is interesting that the C value has also decreased, from 59 to 22. This indicates that the surface properties of the alumina have been

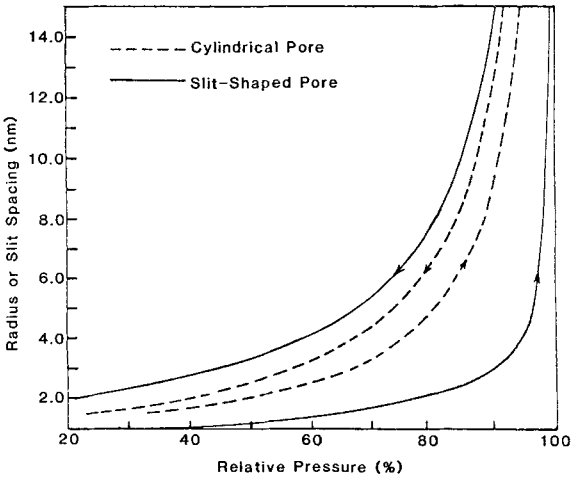

Figure 4. Hysteresis loop gaps predicted from cylindrical and slit-shaped pore models of de Boer.

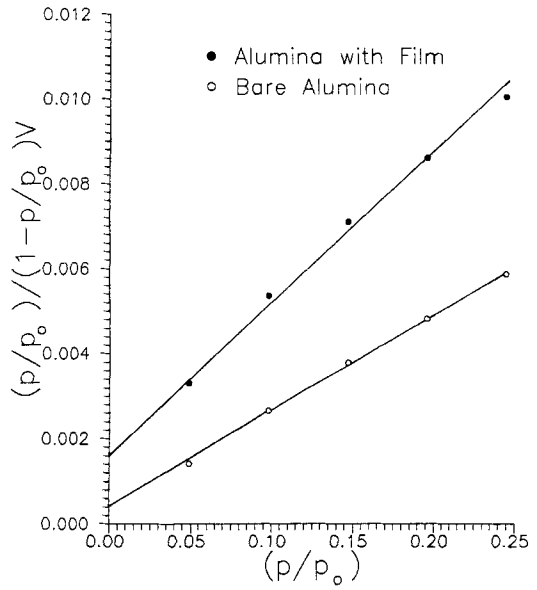

Figure 5. BET plots for modified and unmodified aluminas.

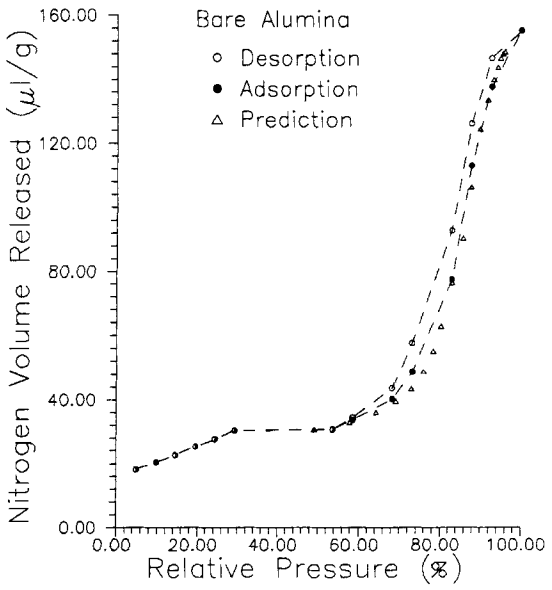

Figure 6. Check of cylindrical pore model applicability to bare alumina by prediction of adsorption branch from a fit of desorption branch.

altered, also. According to Lecloux and Pirard (1979), the C values for certain chlorinated materials are in the range of 40 to 70, while for some organometallic materials the C values are around 20 to 30. A good comparison here is that the surface properties of the treated sample have been shifted from the inorganic-like properties for the bare alumina to organic-like properties by application of the thin film. Note, however, that without a pore distribution analysis it would be impossible to determine whether the decrease in surface area was associated with a uniformly distributed film, or was the result of the closing up of some pores by polymer particles.

A good test of the applicability of a particular pore model to a powder sample is prediction of the adsorption branch of the hysteresis loop from a fit of the desorption branch (Christian and Tucker, 1981a, b). The partial hysteresis loops predicted for the cylindrical pore model for both samples are shown in Figures 6 and 7. The cylindrical pore model clearly provides a good description for the alumina in this study, both with and without the film.

The application of de Boer's theory, using the cylindrical pore model, to the calculation of pore size distribution results in the plots shown in Figures 8, 9, and 10, which respectively show pore volume, pore surface area, and total pore length distributions. Tie lines are shown in Figure 10. The total surface area contributed by the pore walls is 95.7 m^2/g for the bare alumina sample, which is almost the same as the BET surface area. For the film sample, the pore surface area is 78.7 m^2/g, which is about 50% more than the BET surface area. The difference may be attributable to the heterogeneous nature of the pore surface properties after the formation of the thin film; variations of this type in the heat of adsorption of the first layer of gas molecules are not accounted for in the BET analysis. The most important observation to be made from these plots is that the pore size distributions have the same basic shape for the aluminas with and without the film; this indicates that the thin film has uniformly reduced the pore diameters of all of the pores, rather than simply plugging some of the pores. It should also be noted that pores of diameters less than 2.0 nm are not susceptible to analysis by the de Boer model.

Film thickness predicted from pore size distribution curves

To evaluate the ultrathin film thickness, tie lines have to be established to connect points on the original pore size distribution with points on the new pore size distribution. The dashed tie lines in Figure 10, the plot of the total pore length distributions, connect two points, one located on the bare alumina curve and the other on the modified alumina curve. These tie lines have a slope of zero, as discussed above. The film thicknesses corre-

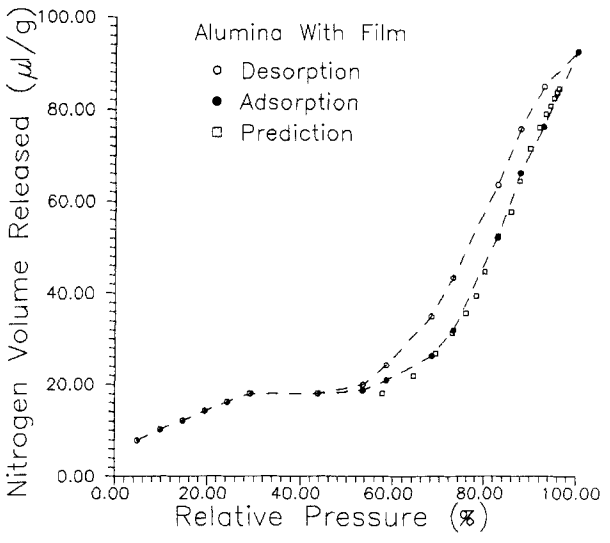

Figure 7. Check of cylindrical pore model applicability to alumina with thin film by prediction of adsorption branch from a fit of desorption branch.

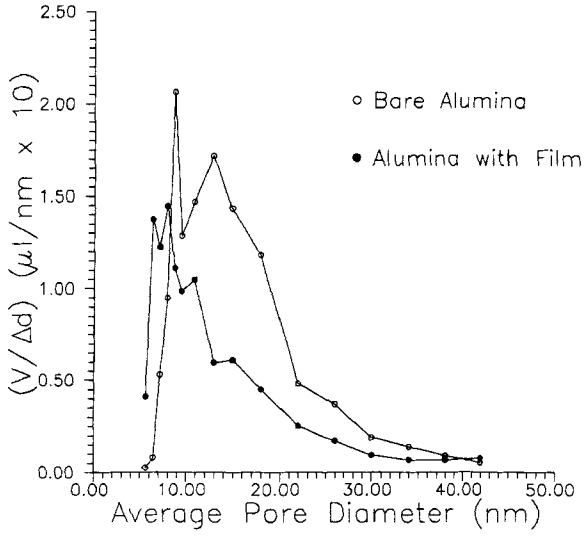

Figure 8. Pore volume distributions for modified and unmodified aluminas for cylindrical pores.

spond to half the difference in the pore diameters between the two points connected by the tie lines.

The results of the calculations of film thicknesses based on a distribution of cylindrical pores for both samples are shown in Figure 11. The same results can be obtained by constructing the tie lines for the other distributions, shown in Figures 8 and 9, using Eq. 1-4. Film thicknesses are seen to vary from 1.8 to 0.4 nm. For larger pores, the apparent film thickness is greater. This may be an artifact of the assumptions of the model, but it may also indicate a more complete coverage of the surface of the larger pores. It is impossible to determine from this analysis whether there is a change in film morphology between the large-diameter pores and the small-diameter pores. The calculated average thicknesses for each pore size can be compared with the overall average thickness calculated from the amount of SDS adsorbed upon the surface of the bare alumina. Based on the amount of surfactant adsorbed on the sample, the surface area

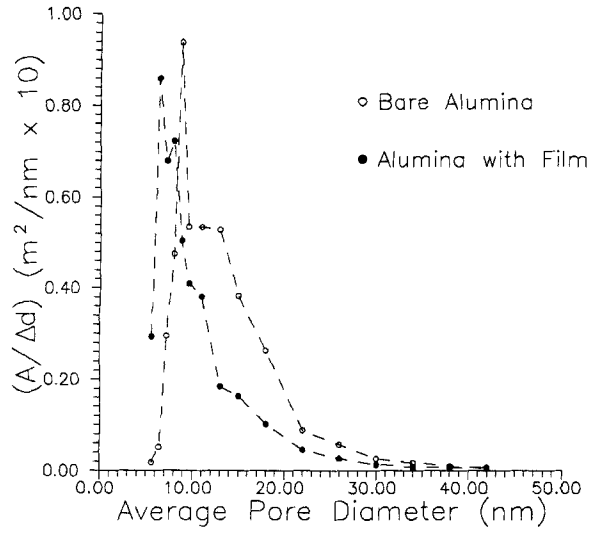

Figure 9. Pore area distributions for modified and unmodified aluminas for cylindrical pores.

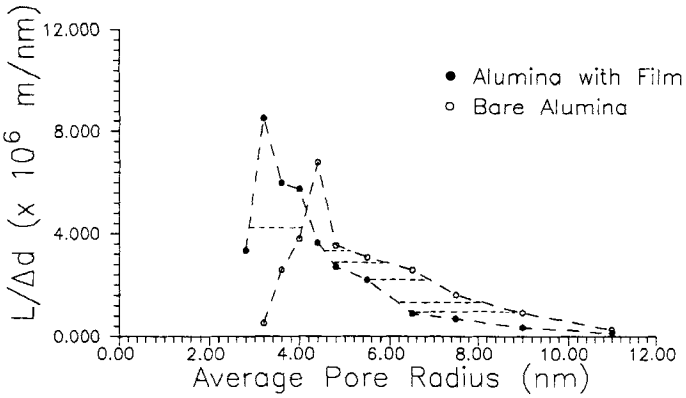

Figure 10. Pore length distributions for modified and unmodified aluminas for cylindrical pores.

of the bare alumina, and the cross-sectional area of the SDS head group, there is approximately 0.55 fractional bilayer coverage at the time of the initiation of the polymerization. This gives an overall average film thickness of around 1.7 nm, which is near the upper limit of the film thicknesses determined from the pore distribution curves. Another comparison comes from the total pore volume determined from the nitrogen sorption isotherm at a 95% nitrogen composition. This yields an average film thickness of 1.0 nm, which is between the 1.8 and 0.4 nm obtained for the cylindrical pore model.

Effect of washing film samples with water

In addition to the results described above, there is another interesting phenomenon associated with the formation of the thin film on the alumina powder, which occurs after washing of the modified samples with water. Bare alumina powders are hydrophilic, and sink spontaneously when placed on the surface of water in a beaker. However, the thin film modified alumina

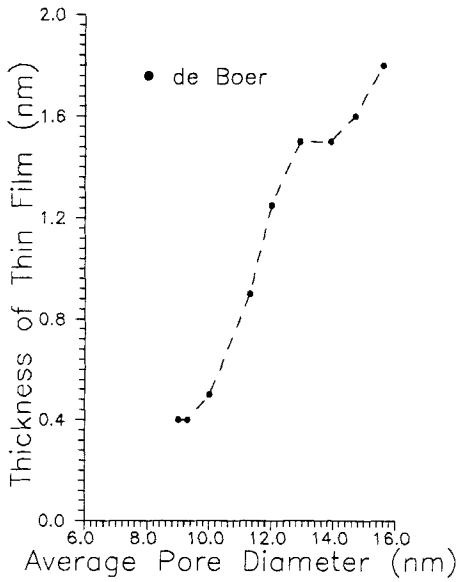

Figure 11. Surface average film thickness as a function of pore diameter.
Results determined from shift in pore size distribution upon application of thin film to alumina.

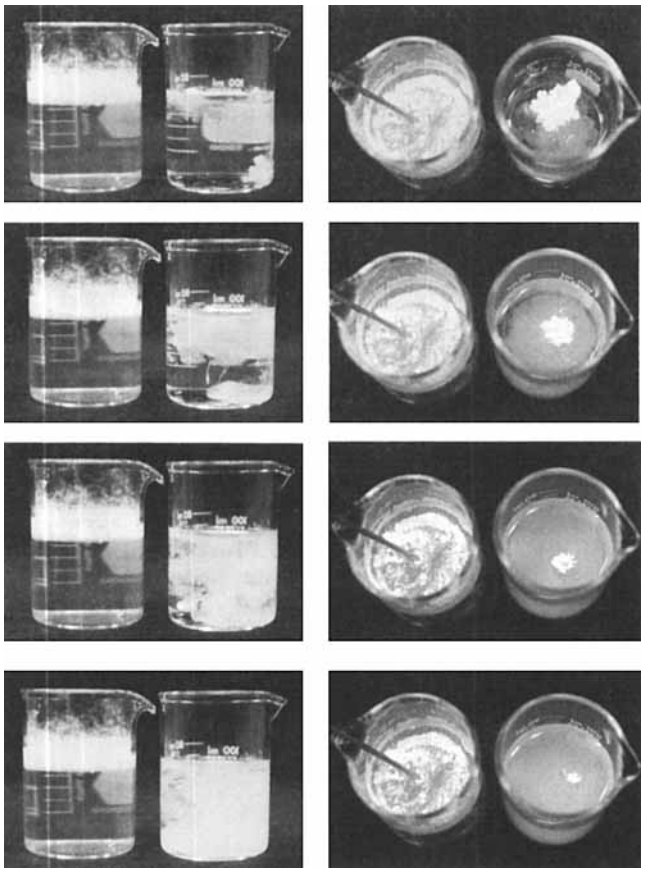

Figure 12. Demonstration of hydrophobicity of modified alumina after washing.

Side and top views of beakers containing water after modified alumina is added to left beaker and unmodified alumina added to right beaker.

exhibits a different behavior. It was found that most of the modified powders, after having been washed with water and then dried in a vacuum oven, will float on a water surface for many months. This behavior is illustrated in Figure 12, where the modified alumina stays atop the water surface, but the bare alumina is immediately dispersed throughout the beaker; if left undisturbed it will soon settle to the bottom. Individual particles of the modified alumina, when forced beneath the water surface with a spatula, immediately pop back above the surface and give every appearance of being completely dry. In contrast, the unwashed alumina/film samples sink into the water easily, just like the bare alumina, even after drying in a vacuum oven. This behavior suggests that the surface of the modified powder is hydrophilic after the polymerization step and before washing, but is hydrophobic after the washing. The polymerization step is subsequent to the adsorption and adsolubilization steps, and the unwashed alumina must retain the original surfactant of the admicelle, with the hydrophilic head groups of the upper SDS layer in contact with the aqueous phase. But once this upper SDS layer is removed (or partially removed) by washing, the underlying hydrophobic surface, which consists of the polystyrene and the tails of the lower SDS layer of the admicelle, changes the contact angle between the powder surface and the water, and prevents water from reentering the pore spaces after it has once been removed by drying. This causes the alumina powders to float on water spontaneously, the air trapped in the pores making the particles less dense than water. If surfactant is added to the water on which the modified powder is floating, it will eventually become wet and sink into the beaker. It appears that, without water washing, the film retains the polymerized SDS admicelle-polystyrene complex. After the water wash, the upper surfactant layer of the admicelle is removed, but the underlying hydrophobic polymer is retained.

Conclusions

1. The surface-averaged film thicknesses, as determined from the nitrogen sorption isotherms, vary with pore diameter from 1.8 to 0.4 nm, based on the cylindrical pore model of de Boer. For a 55% bilayer surface coverage, as determined by observed surfactant adsorption densities, the overall average film thickness is 1.7 nm, which is in good agreement with the thicknesses determined from the sorption data.

2. The ultrathin films, consisting of SDS imbedded in polystyrene, are distributed almost uniformly over the pore surface of the alumina powders. There may be a greater fractional coverage in the larger diameter pores, however. It is impossible to determine from this analysis whether or not there is a change in film morphology in the smaller pores.

3. Depending on whether it is washed or contacted with an aqueous surfactant solution, the alumina surface can be altered from hydrophilic to hydrophobic and back after the application of the film.

4. The cylindrical pore distribution model is a good representation of the pore structure of the alumina employed in the present study, both before and after the application of the thin film. The basic shape of the pore size distribution curves are not changed by the formation of the thin film, but are simply shifted to smaller diameters. This is a further indication that the film formed in the process is of molecular dimensions and is uniformly distributed over the pore surface of the powder.

5. Estimates of the film thickness obtained from the adsorption data of SDS on alumina and from the hypothesized structure of the SDS admicelle with adsolubilized monomer, prior to the polymerization, both agree well with the thicknesses obtained by analysis of the pore size distribution curves.

Notation

A_c = pore surface area for bare alumina, nm^2
A'_c = pore surface area for sample with film, nm^2
r = pore radius, nm
t_f = thickness of ultrathin film inside pores, nm
V_c = pore volume for bare alumina, nm^3
V'_c = pore volume for sample with film, nm^3

Literature Cited

Barrett, E. P., L. G. Joyner, and P. P. Halenda, "The Determination of Pore Volume and Area Distributions in Porous Substances. I: Computations from Nitrogen Isotherms," *J. Am. Chem. Soc.*, **73**, 373 (1951).

Christian, S. D., and E. E. Tucker, "Micropore Distribution Analysis Based on Gas Adsorption I," *Am. Lab.*, **13**(8), 42 (1981a).

———, "Micropore Distribution Analysis Based on Gas Adsorption. II," *Am. Lab.*, **13**(9), 47 (1981b).

Cranston, R. W., and F. A. Inkley, "Determination of Pore Structures from Nitrogen Adsorption Isotherms," *Adv. Catal.*, **9**, 143 (1957).

de Boer, J. H., and B. C. Lippens, "Studies on Pore Systems in Catalysts. II: The Shape of Pores in Aluminum Oxide Systems," *J. Catal.*, **3**, 38 (1964a).

———, "Studies on Pore Systems in Catalysts. III: Pore Size Distribution Curves in Aluminum Oxide Systems," *J. Catal.*, **3,** 44 (1964b).
de Boer, J. H., B. G. Linsen, and Th. J. Osinga, "Studies on Pore Systems in Catalysts. VI: The Universal *t*-Curve," *J. Catal.*, **4,** 643 (1965a).
de Boer, J. H., B. G. Linsen, Th. van der Plas, and G. J. Zondervan, "Studies on Pore Systems in Catalysts. VII: Description of Pore Dimensions of Carbon Blacks by the *t*-Method," *J. Catal.*, **4,** 649 (1965b).
Dubinin, M. M., "Capillary Evaporation and Information on Structure of Adsorbent Mesopores," *J. Colloid Interf. Sci.*, **77,** 84 (1980).
Harwell, J. H., J. C. Hoskins, R. S. Schechter, and W. H. Wade, "Pseudophase Separation Model for Surfactant Adsorption: Isomerically Pure Surfactants," *Langmuir,* **1,** 251 (1985).
Innes, W. B., "Use of a Parallel-Plate Model in Calculation of Pore Size Distribution," *Anal. Chem.*, **29,** 1069 (1957).
Juhola, A. J., and O. W. Edwin, "Pore Structure in Activated Charcoal. I: Determination of Micro Pore Size Distribution," *J. Am. Chem. Soc.*, **71,** 2069 (1949).
Joyner, L. G., E. P. Barrett, and R. J. Skold, "The Determination of Pore Volume and Area Distributions in Porous Substances. II: Comparison between Nitrogen Isotherm and Mercury Porosimeter Methods," *J. Am. Chem. Soc.*, **73,** 3155 (1951).
Lecloux, A., and J. P. Pirard, "The Importance of Standard Isotherms for Determing the Pore Texture of Solids," *J. Colloid Interf. Sci.*, **70,** 265 (1979).
Outlon, T. D., "The Pore Size-Surface Area Distribution of a Cracking Catalyst," *J. Phys. Colloid Sci.*, **52,** 1296 (1948).
Pierce, C., "Computation of Pore Sizes from Physical Adsorption Data," *J. Phys. Chem.*, **57,** 149 (1953).
Pierce, C., and R. L. Smith, "Adsorption-Desorption Hysteresis in Relation to Capillarity of Adsorbents," *J. Phy. Chem.*, **54,** 784 (1950).
Ries, H. E., R. A. Van Nordstrand, F. L. Johnson, and H. O. Brunauer, "Adsorption-Desorption Isotherm Studies of Catalysts in the Powder and Pellet Forms," *J. Am. Chem. Soc.*, **67,** 1242 (1945).
Ritter, H. L., and L. C. Drake, "Pore-Size Distribution in Porous Materials. Pressure Porosimeter and Determination of Complete Macropore Size Distributions," *Ind. Eng. Chem., Anal. Ed.*, **17,** 782 (1945).
Roberts, B. F., "A Procedure for Estimating Pore Volume and Area Distributions from Sorption Isotherms," *J. Colloid Interf. Sci.*, **23,** 266 (1967).
Scamehorn, J. H., R. S. Schechter, W. J. Wade, "Adsorption of Surfactants on Mineral Oxide Surfaces from Aqueous Solutions," *J. Colloid Interf. Sci.*, **85,** 463, 1982.
Wayne, L., "A Method of Obtaining Approximate Pore Size Distribution Curves from Nitrogen Sorption Isotherms," *J. Am. Chem. Soc.*, **73,** 5498 (1951).
Wheeler, A., "Reaction Rates and Selectivity in Catalyst Pores," *Adv. Catal.*, **3,** 250 (1951).
Wu, J., "The Sodium Dodecyl Sulfate Admicelle on Alumina as a Two-Dimensional Solvent for Styrene Polymerization—The Formation and Characterization of Ultrathin Films and Their Application as an Ion-Exchange Material," PhD Diss., Univ. Oklahoma (1987).
Wu, J., J. H. Harwell, and E. A. O'Rear, "Two-Dimensional Solvents: Kinetics of Styrene Polymerization in Admicelles at or near Saturation," *J. Phy. Chem.*, **91,** 623 (1987a).
———, "Two-Dimensional Reaction Solvents: Surfactant Bilayers in the Formation of Ultrathin Films," *Langmuir,* **3**(4), 531 (1987b).
———, "Characterization by Ellipsometry of Polymerized UltraThin Films Formed in a Two-Dimensional Solvent on an Oxide Surface," *Colloids and Surfaces,* **26,** 155 (1987c).

Manuscript received Sept. 25, and revision received Mar. 11, 1988.